Article

FE Analysis of Laser Shock Peening on STS304 and the Effect of Static Damping on the Solution

Ryoonhan Kim [1], Jeong Suh[1], Dongsig Shin[1]*, Kwang-Hyeon Lee[1], Seung-Hoon Bae[1], Dae-Won Cho[1]* and Won-Geun Yi [2]

[1] Busan Machinery Research Center, Korea Institute of Machinery and Materials, Busan, 46744, Republic of Korea; rhkim@kimm.re.kr
[2] Doosan Heavy Industries, Changwon, 51711 ,Republic of Korea; wongeun.yi@doosan.com
* Correspondence: dwcho@kimm.re.kr(D.C.); dsshin@kimm.re.kr(D.S)

Abstract: Laser shock peening is a process which can reduce stress corrosion cracking and improve fatigue life by forming compressive residual stress on the surface of the material. In a computational FE simulation of laser shock peening, during applying the pressure load generated by the laser pulse to the surface of simulation geometry, the peening is simulated by explicit analysis and then convert to implicit analysis to dissipate the dynamic energy remaining in the geometry. In this study, static damping is applied to dissipate residual dynamic energy without converting it into an implicit analysis. The compressive residual stress distribution is compared between the simulation results for the stainless steel 304 material and the same material subjected to actual laser shock peening. The laser shock peening parameters were 4.2J laser pulse energy, 50% overlap of 3mm diameter of the laser beam and water as a confinement layer. As a result, the compressive residual stress from the surface to the depth direction is similar to both the simulation and the experimental result measured by the hole drilling method.

Keywords: Laser shock peening; FE simulation; Residual stress, Minimum principal stress, Static damping

1. Introduction

The peening process, which aims to form compressive residual stress on the surface of the material, improves fatigue life by preventing crack generation and propagation. It also delays the stress corrosion cracking, where the tensile residual stress is existing like welded metal, by forming compressive residual stress on the material. Peening process includes shot peening, ultrasonic peeing, etc. However, both processes largely deform the material surface and generate the compressive residual stresses within a few micrometers of the surface. Laser shock peening(LSP) is known to improve fatigue life by 4 to 5 times compared to other peening processes by forming compressive residual stress to a depth of several millimeters from the surface, unlike other peening processes. LSP is one of a material surfacing process for forming compressive residual stress on the surface of a material using a plasma shock wave generated by the reaction between a high-energy laser pulse and a material[1]. When the plasma pressure shock is applied on the material surface, the laser beam irradiated area deform plastically and pushes near material. As an interaction, the elastic region pushes back to the plastically deformed zone, and the compressive residual stress remains. The compressive residual stress and grain refinement generated by laser shock peening are known to increase stress corrosion cracking resistance and fatigue life of the alloy[2,3]. However, LSP is mainly applied to high value-added products because the process cost is high compared to other peening processes[4]. There are cases where LSP has been applied to unique parts subject to fatigue loads such as turbine blades of aircraft and helicopter drive train gears, and to prevent corrosion cracking of welded parts in nuclear reactors[5].

FEM analysis of LSP, began with Ballad[6], there were several researches which used an *ABAQUS* based simulation[7–12] and *ANSYS LS-DYNA* based[13–15] simulation. The LSP process is usually done within an instant time. The plasma pressure loading takes less than 200ns and the material plastically deformed after. Due to this process characteristic, FE simulation of the LSP was analyzed with the explicit method. The explicit analysis is considered in case of a non-linear problem like plastic deformation simulation but takes much more calculation time than implicit analysis due to its small timestep size. To settle static-equilibrium state, import the explicit analysis result to implicit analysis and it was repeated until to final loading as shown in Figure1[16].

Peyre et al[8] performed LSP FE simulation of 12% Cr stainless steel based on the strain rate dependent stress-strain relationship as Johnson-Cook model. Two steps analysis was repeated for every single shot, 1st step was loading and 2nd was calculating the deformation and residual stress field. However, there was a disadvantage that it took 1ms calculation time to wait for stabilization and as a result, it spent one-hour wall-clock per shot. Amarchinta et al[9] conducted LSP FE simulation of Ti–6Al–4V material by using Johnson and Cook and Zerilli and Armstrong stress-strain models. Depending on the laser pulse energy, residual stress was evaluated according to depth. As a simulation method, the pressure was applied through dynamic loading analysis, and residual stress was analyzed through static equilibrium analysis. As shown in the Figure1, Hasser et al[17] proposed a SEATD analysis method to obtain a rapid stabilization state using damping after loading period without switching to implicit analysis. This method was performed six times faster total calculation time than the 2N+1 analysis method which proposed Brockman et al[18]. Bahmare et al[15] used *LS-DYNA* simulation tool with Zerilli and Armstrong model, LSP FE simulation of the material Ti–6Al–2Sn–4Zr–2Mo. Only explicit analysis was applied with damping for stabilization, but the damping value was not described in detail.

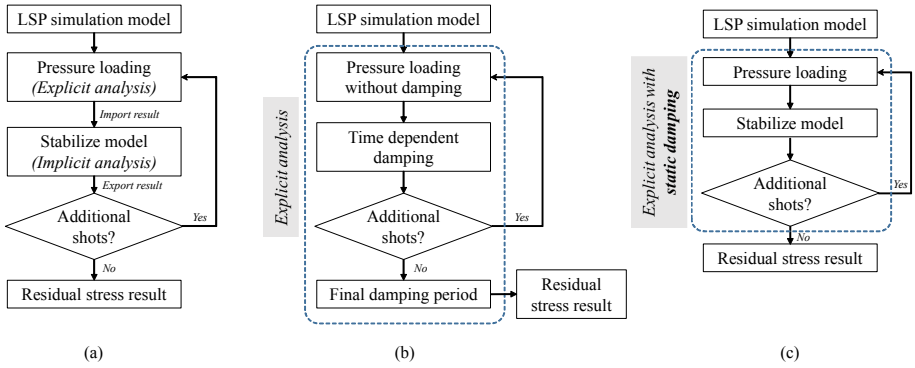

Figure 1. Analysis flow chart: (**a**)Typical explicit and implicit method; (**b**) SEATD explicit method; (**c**) Proposed static damping explicit method.

In this study, different from other research, the static damping is applied also in loading and relaxation period. The effect of the static damping value is evaluated from single LSP and overlapped multiple LSP simulation result. The comparison of the residual stress of the laser shock peened material and the LSP simulation results are discussed.

2. LSP Process Modeling

2.1. Conservation Equations for Explicit Analysis

The partial difference equations(PDE) of expressed as mass, momentum, energy conservation to be solved in explicit solver. The FE model, boundary condition, initial condition and loading condition are also calculated. Each conservation equations are expressed as[19],

Mass conservation equation:

$$\frac{\rho_0 V_0}{V} = \frac{m}{V} \tag{1}$$

Momentum conservation equation:

$$\begin{aligned} \rho\ddot{x} &= b_x + \frac{\delta\sigma_{xx}}{\delta_x} + \frac{\delta\sigma_{xy}}{\delta_y} + \frac{\delta\sigma_{xz}}{\delta_z} \\ \rho\ddot{y} &= b_y + \frac{\delta\sigma_{yx}}{\delta_x} + \frac{\delta\sigma_{yy}}{\delta_y} + \frac{\delta\sigma_{yz}}{\delta_z} \\ \rho\ddot{z} &= b_z + \frac{\delta\sigma_{zx}}{\delta_x} + \frac{\delta\sigma_{zy}}{\delta_y} + \frac{\delta\sigma_{zz}}{\delta_z} \end{aligned} \tag{2}$$

Energy conservation equation:

$$\dot{e} = \frac{1}{\rho}(\sigma_{xx}\dot{\varepsilon}_{xx} + \sigma_{yy}\dot{\varepsilon}_{yy} + \sigma_{zz}\dot{\varepsilon}_{zz} + 2\sigma_{xy}\dot{\varepsilon}_{xy} + 2\sigma_{yz}\dot{\varepsilon}_{yz} + 2\sigma_{zx}\dot{\varepsilon}_{zx}) \tag{3}$$

Here, ρ is density;V is volume; m is mass; b is momentum term; σ is stress tensor term; e is energy term; and ϵ is strain.

2.2. Static Damping

The *ANSYS Explicit Dynamics* solver is used to solve transient analysis. Using the static damping option, a static equilibrium solution can also be obtained. *ANSYS* presents a guideline for the proper static damping value[20,21]. The procedure introduces a damping force that is proportional to nodal speed and aims to critically damped the lowest vibration mode of a static system. When damping value option is used, the nodal velocity is calculated every iteration in solver as Equation4

$$v^{n+1/2} = (1 - 2\pi R_d)v^{n-1/2} + (1 - \pi R_d)\dot{v}\Delta t^n \tag{4}$$

Where v is the nodal velocity, R_d is a static damping value, Δt is a time step during solved.

$$R_d = \frac{2\Delta t/T}{1 + 2\pi\Delta t/T} \tag{5}$$

Here, T is the period of the lowest mode of vibration. The values of Δt and T are can be obtained by after first solve of the FE model without damping option. These values should be estimated by user and T should not be underestimated. The values that used in this study be discussed later.

2.3. Stress-Strain Model

Every material has their own stress-strain curve. These curves were mostly optained by tensile tests. However, LSP process deforms material surface with high speed and in case of high strain rate(strain per time) process, stress-strain curves are changing depending on the strain rate. There are several model of high strain rate stress-strain relationship well known as Johnson-Cook(JC)[22], Zerilli-Amstrong(ZA)[23] and Khan-Huang-Liang(KHL)[24] equation.

$$\sigma = [A + B(\varepsilon)^n][1 + Cln(\dot{\varepsilon})][1 - T^m] \tag{6}$$

Equation (6) is JC model, where A, B, C, n and m are the material dependent coefficients that determined by experiment. A is the yield strength; B is hardening modulus; C is strain rate dependency coefficient; ε is the effective plastic strain; $\dot{\varepsilon}$ is the effective plastic strain rate; n is the work hardening exponential; m is the term of thermal softening[25]. Thermal term of JC model is neglected because the LSP is regarding as a non-thermal process[11,14,26]. JC model is used in this study for FE simulation.

2.4. Pressure Load Model

Plasma pressure shock induced by the interaction between the material and the high-energy laser pulse need to be applied on the surface of the simulation geometry. Several pressure loading models were proposed in previous studies. The pressure load was expressed as a function of time, simple triangular load model[13] and expressed as a step load model[14]. Langer et al[26] proposed that the impedance of water confinement term and the pressure load which converted by laser energy were expressed as a function of time[26]. The pressure load applied in this work is shown in Figure2. This normalized pressure load model was proposed by several research[9,27].

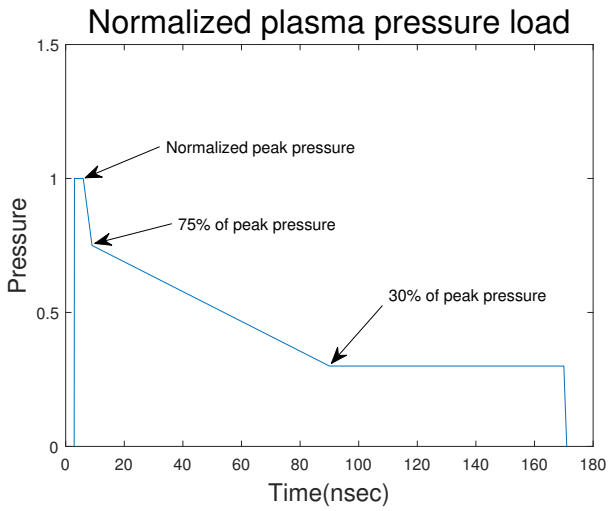

Figure 2. Normalized pressure load profile.

The peak pressure can be calculated as Equation(7). Here, $P_{peak}(GPa)$ is the peak plasma pressure; α is the correction factor of the internal energy and the thermal energy(usually $\alpha \approx 0.25$); $I(GW \cdot cm^{-2})$ is the laser pulse power density where P_{pulse} is laser pulse power and A_{peen} is laser pulse area at working point; $Z(g \cdot cm^{-2}s^{-1})$ is the combined acoustic impedance of confinement layer $Z_{water}(\approx 0.15 \times 10^6)$ of water and target material $Z_{target}(\approx 4.5 \times 10^6)$ of stainless steel[8,12,28,29].

$$P_{peak} = 0.01\sqrt{\frac{\alpha}{2\alpha + 3} \cdot Z \cdot I} \tag{7}$$

$$\begin{aligned} \frac{2}{Z} &= \frac{1}{Z_{water}} + \frac{1}{Z_{taget}} \\ I &= \frac{P_{pulse}}{A_{peen}} \end{aligned} \tag{8}$$

Additionally, 2-D pressure load distribution from the beam center to radial direction is also considered. Depending on the laser beam pulse profile, Gaussian and flat-top models were suggested[12]. Sun et al[30] proposed a mixed shape of Gaussian and flat-top according to the measured from the beam profiler and the other was 80% of peak pressure at the center of the beam and gradually increase to peak pressure till the 0.8 of beam diameter[9,27]. In this work, the flat-top spatial energy laser beam is used as an LSP experiment, radial direction pressure distribution in FE simulation is constant respectively.

2.5. Overlapped Multiple LSP

LSP is usually done by overlapping each single laser pulse to treat the material surface. In this work, both experimental and analytical LSP conditions are set as 50% overlapped as Figure3.

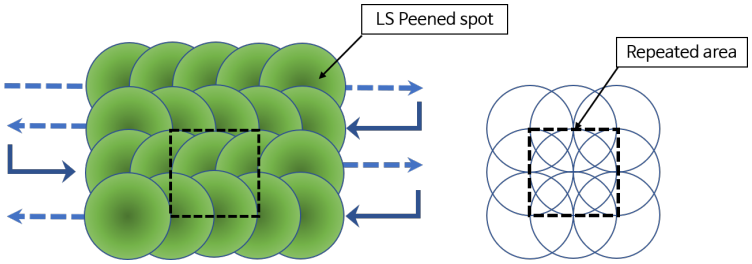

Figure 3. Example of the overlaped multiple LSP pattern.

The laser beam is overlapped in a horizontal direction and also 50% vertically. Through this iterative process, the regions in dotted box of Figure3, are formed repeatedly. In this LSP simulation, to reduce the computational time, nine single LSP pressure loads are applied and the cross-section of repeated area is evaluated.

3. Experiment and FE Analysis Condition

3.1. LSP Experiment Setup

In order to verify FE simulation results, the LSP experiment is done with conditions as shown in Table 1.

Table 1. LSP process variables.

Laser pulse energy *(J)*	Laser pulse width *(ns)*	Beam diameter *(mm)*	Overlap *(%)*	Repetition rate *(Hz)*	Laser type & wavelength *(nm)*	Beam shape	Overlay
4.2	10	3	50	1	Nd:YAG, 1064	Flat-top	Water

Continuum Powerlite Furie is used as a laser system, the laser pulse energy is measured by *Gentec-EO Maestro* console with *QE65LP-H-MB-QED-D0* sensor and the beam diameter is checked by burn paper pattern with low-level pulse energy at the working point. An actual LSP experimental setup is shown in Figure4. The beam-focusing-head focuses 20mm diameter of input beam to increase the energy density and depending on the working distance, LSP spot size can be adjusted. The robot moves the specimen and water is supplied near the working point to form the 1mm thickness of confinement layer. The specimen dimension is 50×40×10mm of stainless steel and the surface is ground condition.

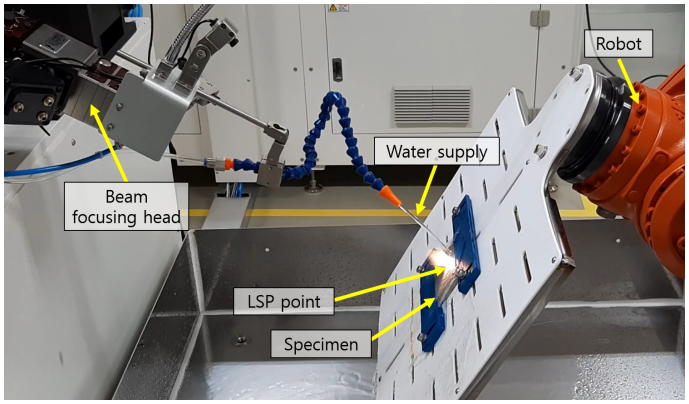

Figure 4. LSP experiment system setup.

3.2. LSP FE Simulation Setup

ANSYS mechanical software is used for LSP FE simulation and for the explicit dynamic analysis, *Autodyn* is set as a solver target. Coordinate system, pressure loading and boundary condition are shown in Figure5.

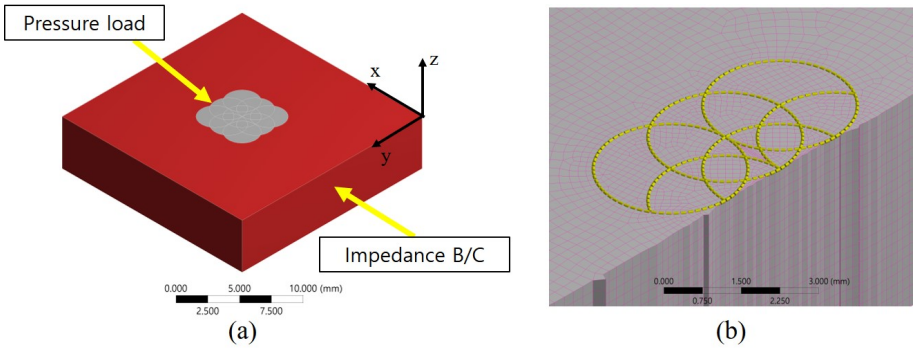

Figure 5. FE Model setup; (a)Pressure load and boundary condition; (b)Edge Sizing.

The dimension of geometry is 20×20×5mm and the X-Y plane is parallel to the top plane of the geometry and the Z axis is parallel to thickness direction respectively. Gray-colored nine circles are the surfaces where the pressure loads are applied according to LSP process modeling setting and the 6 faces (top, bottom and 4-sides) shown in red are set to impedance boundary condition.

Impedance boundary condition allows propagating traveling waves to outward direction of geometry and so the energy not reflecting back into FE geometry. Impedance value is set to zero, it represents the case of perfect transmission of plane normal elastic waves[21].

The propagating elastic wave did not affect the simulation result and also the specimen dimension which used in the experiment is larger than the simulation model, the impedance boundary condition is appropriate. For meshing the simulation geometry, the edges of the circles where the pressure loads applying, are evenly divided into 72 edges and the element size is 0.15mm for fine mesh generation as shown in Figure5. The Multizone meshing method is applied to make a coarse mesh which an element size of 0.25mm where the pressure loads do not applying. Hexa mesh type is selected and other options are left as program-controlled. The material properties are listed in Table 2[31].

Table 2. Material constants of STS304 and coefficients for JC model coefficients.

Material	Density (Kg/m^3)	Poisson's Ratio	Young's Modulus (GPa)	Yield Strength (MPa)	A (MPa)	B (MPa)	C	n
STS304	7750	0.31	200	207	310	100	0.07	0.65

From the Table2 and the Equation7 and 8, the pulse power density of the laser beam I is calculated as $5.94GW \cdot cm^{-2}$ and the P_{peak} as $3.5GPa$ accordingly. The pressure load profile is shown in Figure6. Pressure load is sharply increased to peak pressure($3.5GPa$) in $3ns$, maintained $3ns$, droped to 75% of peak pressure($2.6GPa$) in $3ns$, decreased to 30% of the peak pressure($1.0GPa$) in $81ns$ and keeped during $80ns$ and then drop to 0

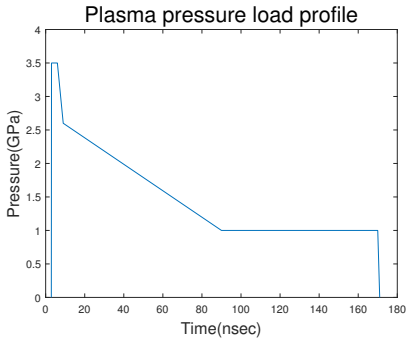

Figure 6. Plasma pressure load model.

To input the pressure loads on the surface of the geometry where the load is applied must be bounded to separate faces. To apply the overlapped loads for simulation, the surface plane is divided into 40 regions and the pressure loads are applied sequentially as shown in Figure7. For example, in the case of the yellow-color-highlighted surface No.16 in Figure7, totally four pressure loads should be applied. If the laser pulse period is $10\mu s$, the loads shall be applied 1st($t = 0$), 2nd($t = 10\mu s$), 5th($t = 40\mu s$), and 6th($t = 50\mu s$) time, repectively. For each face, loading timing is made in order of pressure loading sequence. However, each number in Figure7 is given for convenience and is independent of the order in which pressure loads are applied.

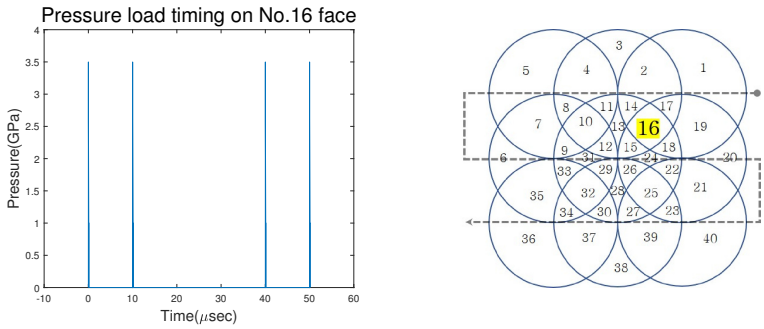

Figure 7. Example of the overlapped multiple LSP pattern. Gray-colored dotted line means the sequence of the pressure loads.

Static damping value R_d is evaluated as 4.6×10^{-5} from the Equation5 by running analysis of the FE model without static damping option. In this study, R_d is selected as 0, 4.6×10^{-5} and others to compare how the static damping affects the result of the deformation and minimum principal stress distribution. Each pressure loading period is $10\mu s$ and the simulation is done with explicit analysis only.

4. Results and Discussion

4.1. Single LSP FE Analysis

4.1.1. Energy Summary

Figure8 shows the each energy variation according to time. The total energy of the pressure pulse load is converted into the internal energy, kinetic energy and hourglass energy. Hourglass energy cannot exist in practice but for calculation stability, it exist when solve the problems which deform with high velocities[13]. In order to estimate the stabilization time depending on the static damping value R_d, differential of internal energy is also plotted. In case of the static damping R_d=0, it converged to zero with variation. Stabilization time for no-damping model is assumed to $10\mu s$ and for multiple LSP simulation, period of each single shot is also set to $10\mu s$. Because, at $10\mu s$ on the kinetic energy graph, remained kinetic energy is relatively small enough, compare to the kinetic energy converted from the pressure loading instance. If it affect the multiple LSP simulation, the solution of no-damping model can diverge or the result shows far different from others which using static damping. In case of $R_d = 4.6 \times 10^{-5}$, the variation of internal energy is existed before $6\mu s$ but after it converged to zero. $R_d = 50 \times 10^{-5}$, it only takes $2\mu s$ to stabilized without variation of the internal energy. The model without damping showed the largest internal energy. The reason is that the applied pressure load is mostly converted into internal and kinetic energy without energy loss due to static damping. However, static damping is needed to make a model absolute-stable-state.

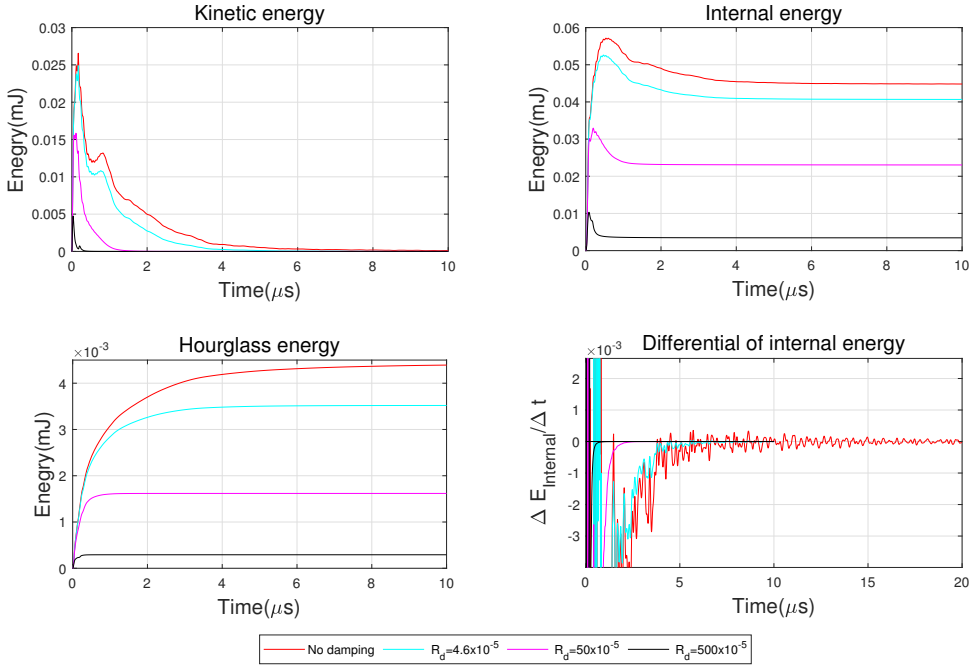

Figure 8. Energy summary of solution. The differential of internal enegry($\Delta E_{Internal}/\Delta t$) is plotted to evaluate the stabilizing time for each damping value.

4.1.2. Transient Analysis

Since LSP is done within a few microseconds, by performing transient simulation, the LSP process can be visualized. Figure9 shows the z-directional deformation change at every $0.2\mu s$ with without damping. Pressure load is delivered to geometry within $0.16\mu s$ as shown in Figure6. However, deformation due to pressure loading continues even afterward. After pressure loading, the maximum amount of deformation appears at $t = 0.5\mu s$ about $0.3\mu s$ passed after loading, and the deformation occurs continuously in the downward direction of the geometry. After $1.1\mu s$, plastic deformation is completed and vibration is gradually stabilized.

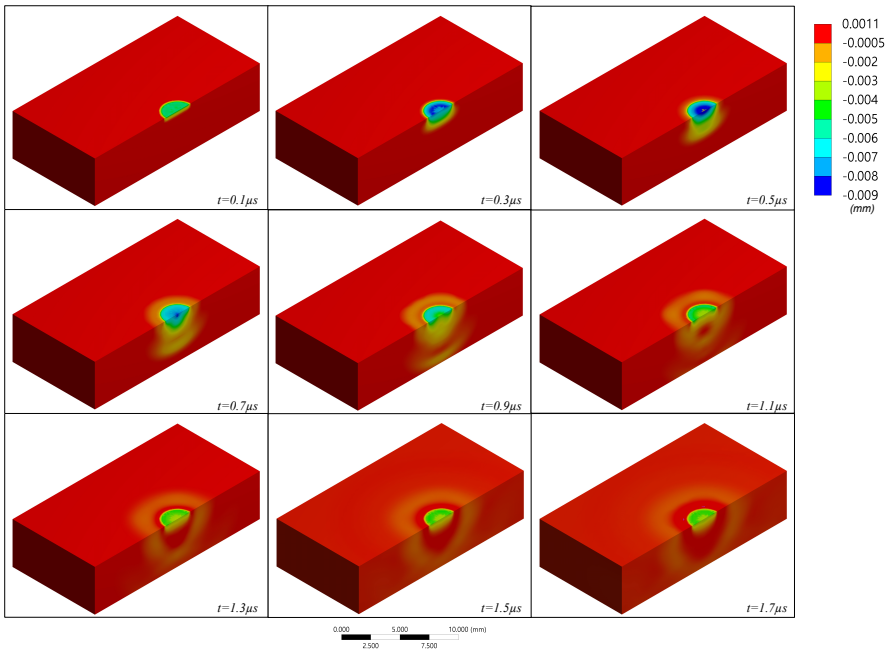

Figure 9. Transient analysis of the Z-directional deformation in single LSP.

4.1.3. Deformation Distribution

To evaluate the Z-directional deformation of the LSP surface, the cross sections of middle of the simulation results depending on the R_d values are plotted as Figure 10. Z-directional deformation values are sampled at the top of the surface. As shown in Figure11, the center of the LSP is slightly less deformed than the surrounding area, while the part where the LSP load is not applied has a surface rising. In case of the large damping value, relatively small deformation is observed.

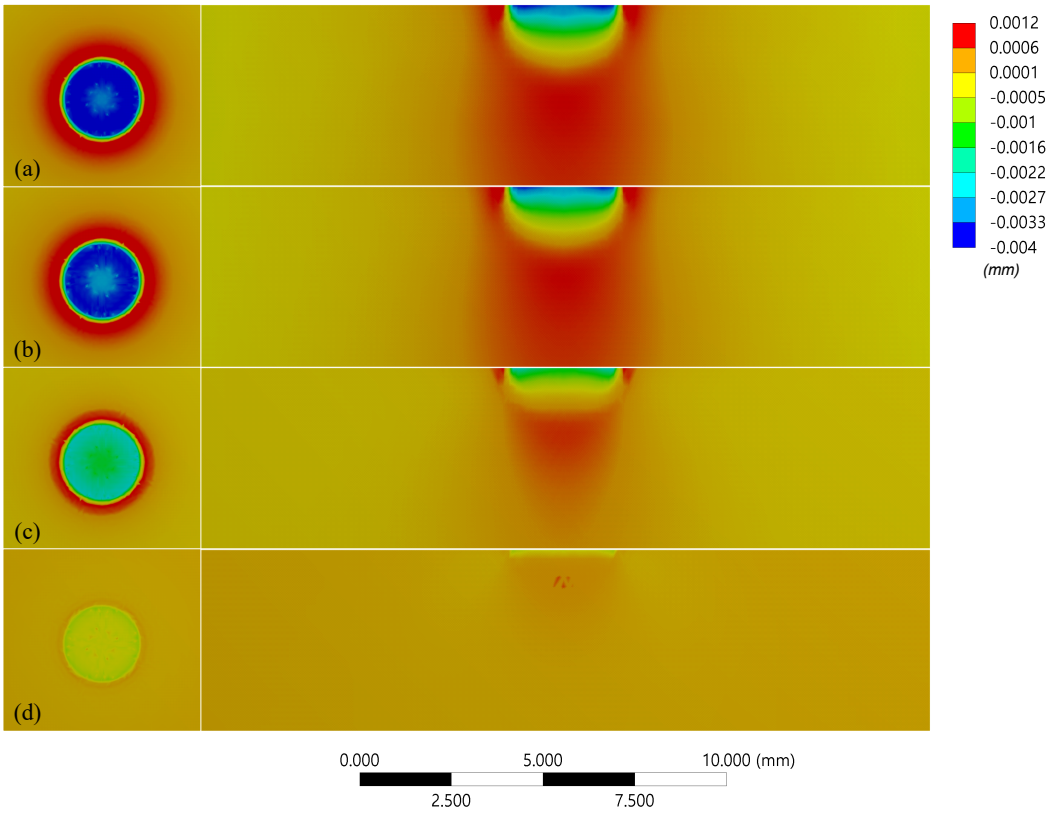

Figure 10. Z-directional deformation of single LSP FE solution. Cross section view on y-z plane; (a)R_d=0; (b)$R_d = 4.6 \times 10^{-5}$; (c)$R_d = 50 \times 10^{-5}$; (d)$R_d = 500 \times 10^{-5}$.

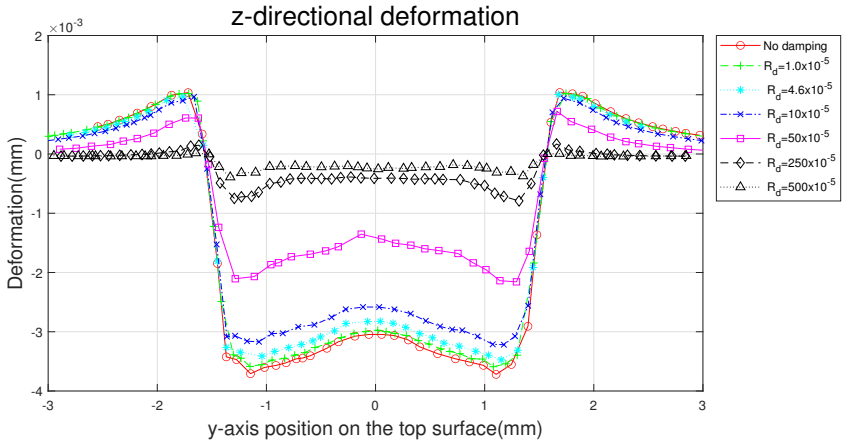

Figure 11. Z-directional deformation distribution on the top surface.

4.1.4. Minimum Principal Stress Distribution

The minimum principal stress distribution of the cross section is shown in Figure12. When overlapped and complicated multiple LSP are simulated, scalar invariant quantity

like minimum principal stress is the best practice to derive meaningful information from simulation[18]. To compare the damping effect, the minimum principal stress value is sampled in the -Z direction from the center point of the LSP as shown in Figure13. The distribution of minimum principal stress in the depth direction, large compressive stress is formed on the surface in the case of large damping values but relatively shallow. In contrast, deep compressive stress is achieved in case of none or small damping is used. Exceptionally, from the Figure12(d), there are few amount of stress distribution near surface. This is due to the large damping extremely reduces the energy which converted from the pressure load.

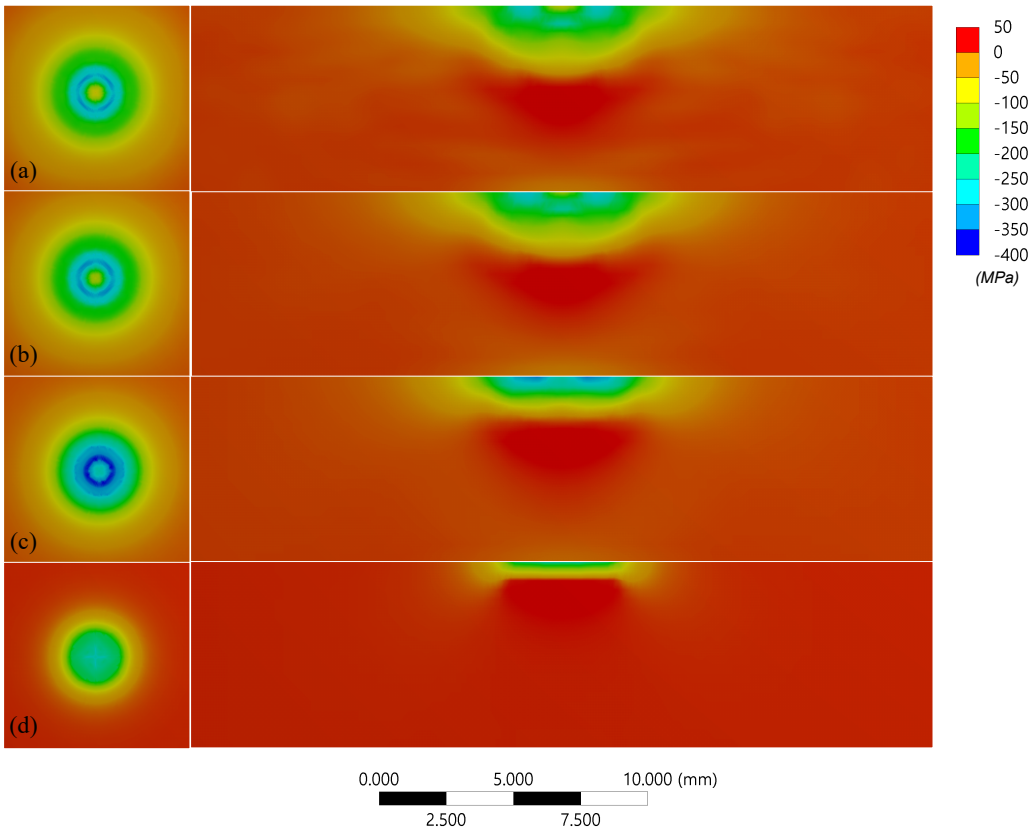

Figure 12. Minimum principal stress of single LSP FE solution; (a)R_d=0; (b)$R_d = 4.6 \times 10^{-5}$; (c)$R_d = 50 \times 10^{-5}$; (d)$R_d = 500 \times 10^{-5}$.

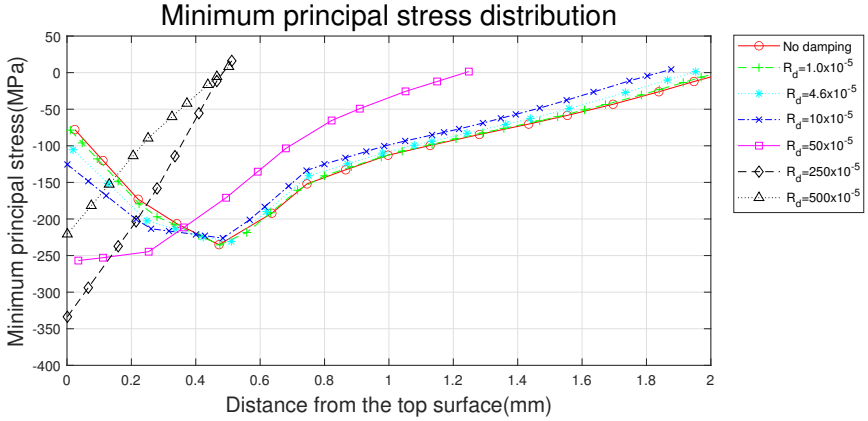

Figure 13. Minimum principal stress of single LSP FE solution.

4.1.5. Discussion on Single LSP FE Analysis

From the energy summary in Figure8, when the static damping value is large, the kinetic energy is quickly dissipated and the time for deformation is short, so that the amount of deformation is relatively small. It is expected that kinetic energy is concentrated on the surface without being transferred in the depth direction for a short period of time, relatively large minimum principal stress is intensively formed near the surface. From the Figure10 through 13 it is commonly observed that the center of the single LSP has small deformation and minimum principal stress but increases along the radial direction. But exceptionally in case of large damping, minimum principal stress at the center is the largest.

Table3 and Figure14 shows the static damping effect on the single LSP simulation result. To easily compare, all values are normalized based on the result of $R_d = 0$. As expected, when increase the damping value on simulation, the model can quickly stabilize but the difference of the deformation and minimum principal stress result getting larger compare to the in case of $R_d = 0$. With $R_d = 4.6 \times 10^{-5}$, simulation time can be reduced to 60% within 10% different from no-damping result. This means that static damping value $R_d = 4.6 \times 10^{-5}$ evaluated from Equation5 is reasonable. Appropriate static damping can be more effective when conduct multiple LSP simulation because it can save the calculation time for every single shot.

Table 3. Simulation result differences depending on the static damping.

Static damping value($\times 10^{-5}$)	Time for stabilization	Maximum depth of minimum principal stress	Maximum deformation on the surface
0	1.00	1.00	1.00
1	0.90	0.95	0.97
4.6	0.61	0.90	0.94
10	0.50	0.87	0.86
50	0.20	0.57	0.58
250	0.10	0.24	0.21
500	0.06	0.22	0.10

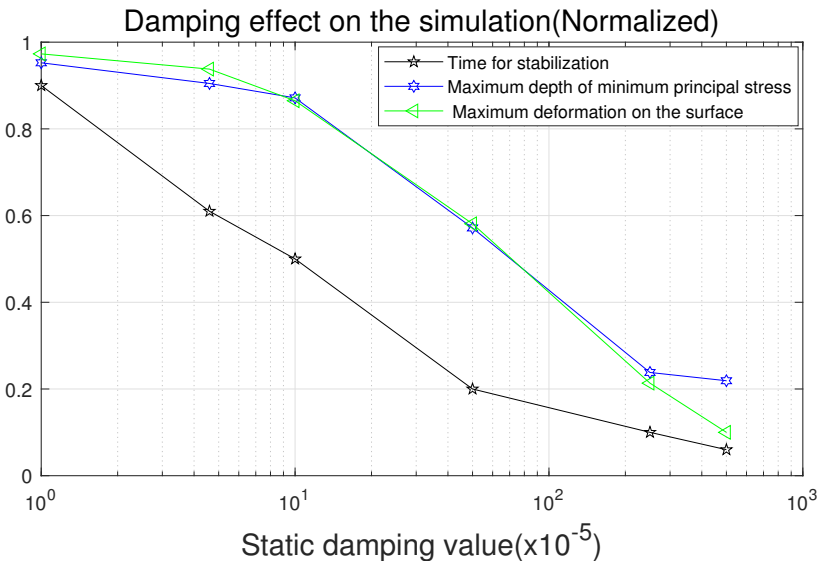

Figure 14. Normalized effect on the FE simulation according to static damping value.

4.2. Multiple LSP FE Analysis

4.2.1. Deformation Distribution

Z-directional deformation values are sampled in the same manner of single LSP analysis. The face No.10, 16, 25 and 32 deforms mostly as shown in Figure16 because of

the four-times overlapped pressure loading. Similar with single LSP result, with large static damping, deformation is small compare to other.

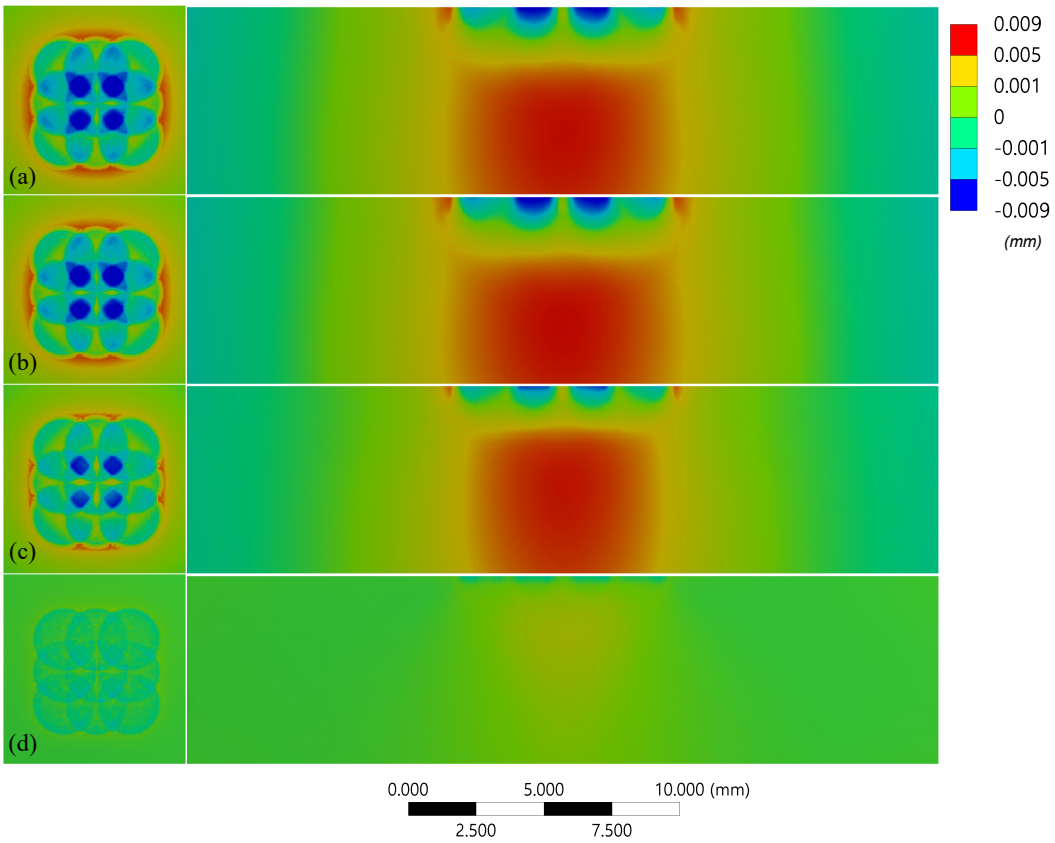

Figure 15. Z-directional deformation of multiple LSP FE solution. Cross section view on y-z plane. (a)R_d=0; (b)$R_d = 4.6 \times 10^{-5}$; (c)$R_d = 50 \times 10^{-5}$; (d)$R_d = 500 \times 10^{-5}$.

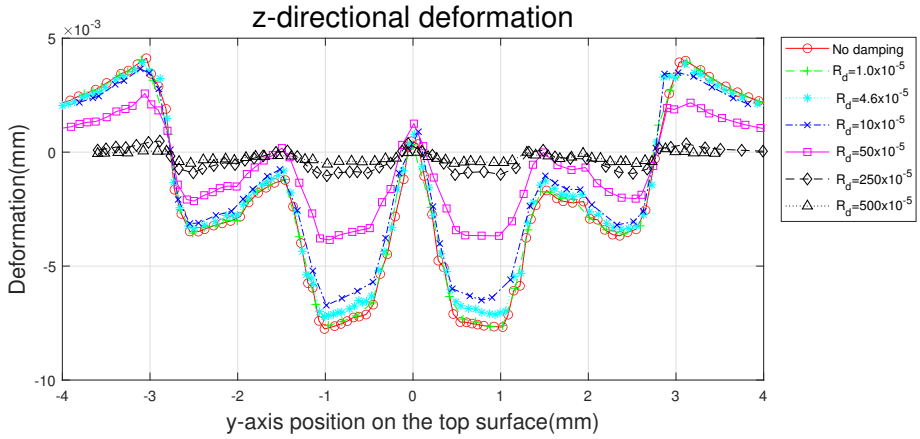

Figure 16. Z-directional deformation distribution on the top surface of multiple LSP FE solution.

4.2.2. Minimum Principal Stress Distribution

The minimum principal stress distribution of multiple LSP FE simulation is shown in Figure18. Compared to single LSP result, it shows similar distribution depending on the static damping. With large value of static damping, even though pressure loads are overlapped, minimum principal stress is not formed deeply but is formed intensively near-surface of the geometry. Similar to single LSP result, with extremely large damping, small minimum principal stress is form at near surface.

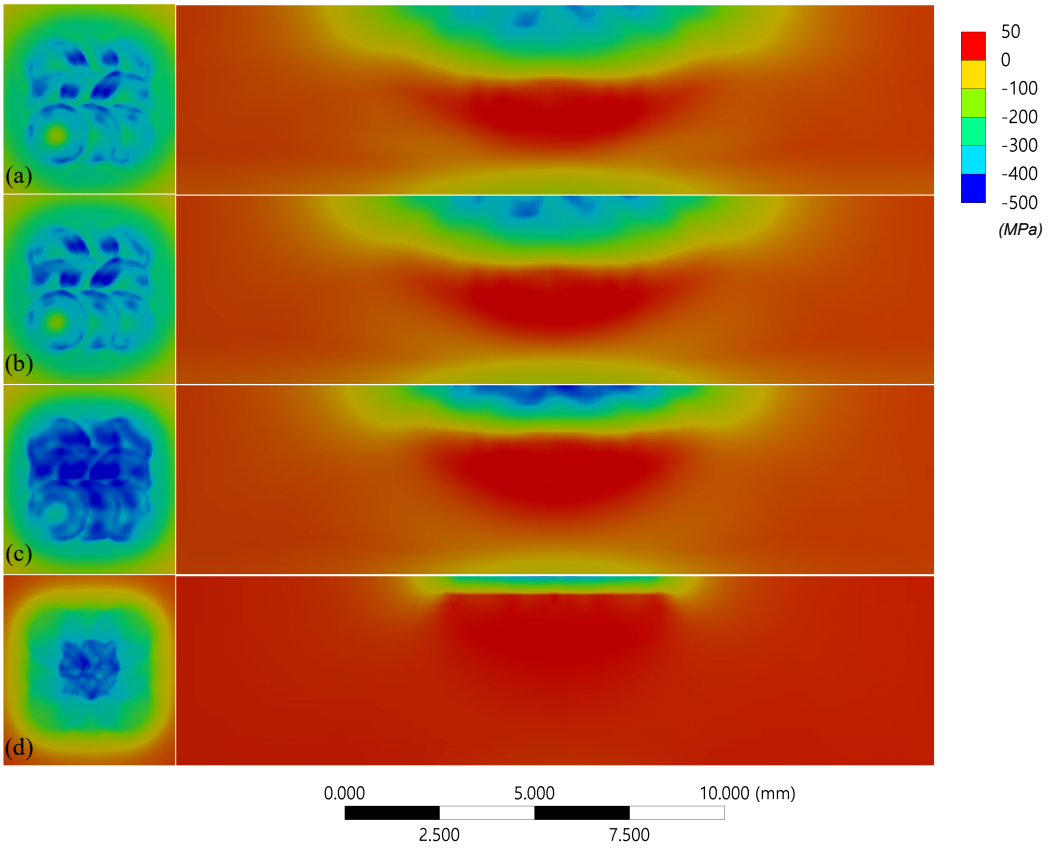

Figure 17. Minimum principal stress of multiple LSP FE solution; (a)R_d=0; (b)$R_d = 4.6 \times 10^{-5}$; (c)$R_d = 50 \times 10^{-5}$; (d)$R_d = 500 \times 10^{-5}$.

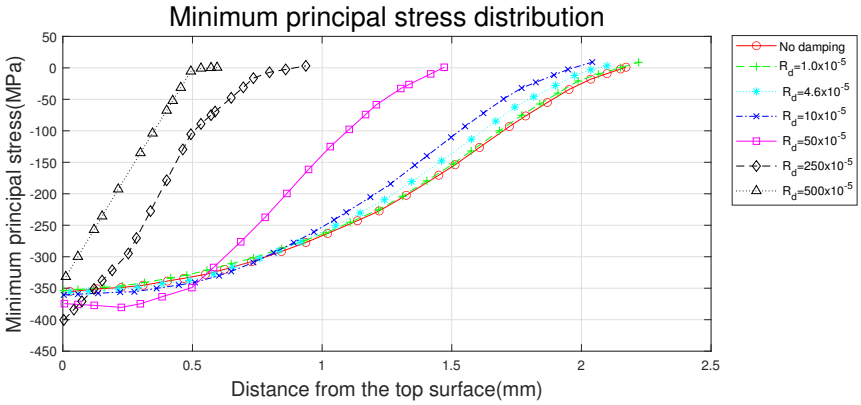

Figure 18. Minimum principal stress of multiple LSP FE solution.

In case of the multiple LSP FE simulation, the effect of the static damping shows similar to a single LSP simulation. As the pressure loads are overlapped, the amount of the deformation and the minimum principal stress are increased respectively. It is confirmed that laser pulses should be overlapped to maximize the LSP effect.

From the deformation and stress analysis result of multiple LSP, no-damping simulation is not diverged and the result is not much different from others. This means even though there exist small kinetic energy in the model, before next shot, it does not effect the solution of the LSP simulation.

4.3. Residual Stress Distribution of LSP Material

To verify the simulation results, the residual stress of the actual LSP-treated specimen is measured by the hole drilling method. The main purpose is to determine whether compressive residual stress was formed up to a depth of 1 mm. Accordingly, the residual stress is measured up to a depth of 1 mm at the center of the LSP test specimen. Test conditions are listed in Table4

Table 4. Hole drilling test parameters for residual stress measurement.

Material	Method	Analysis method	Hole step	Step method	Hole depth(mm)	Analysis step	Analysis step method	Analysis depth(mm)
STS304	Hole drilling	ASTM E837-13	24	Linear	1.2	20	Linear	1

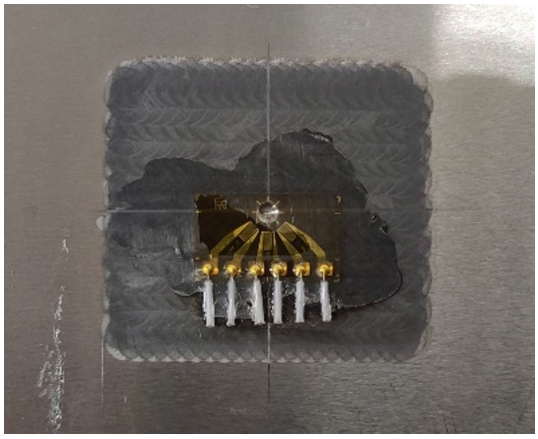

Figure 19. Residual stress measurement of the LSP specimen.

To derive the residual stress, normal stress σ_x and σ_y are analyzed in depth direction at face No.16. Figure20 shows the residual stress distribution on the solution geometry surface.

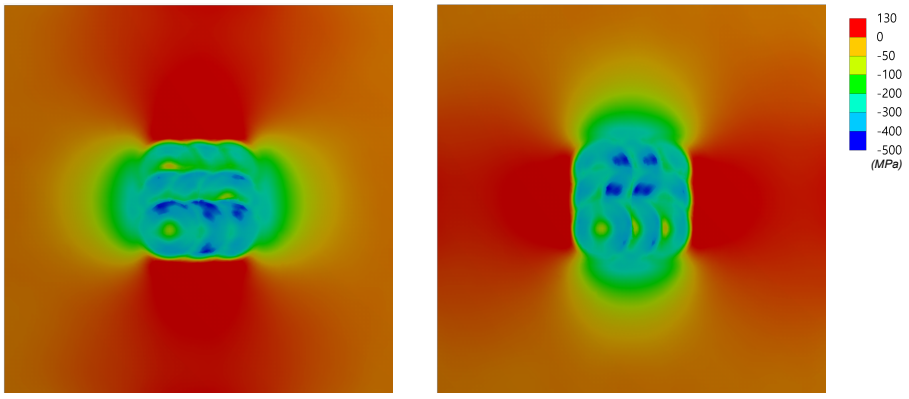

(a) (b)

Figure 20. Residual stress of the geometry surface; (a)normal stress σ_x and (b)normal stress σ_y.

The residual stress(σ_x and σ_y) results of the specimen and the simulated geometry according to depth are plotted as Figure21. It shows that the distribution of compressive residual stress of FE simulation and the experimental result is similar in case of $R_d = 0$ and $R_d = 4.6 \times 10^{-5}$. The residual stress distribution which expressed as σ_x and σ_y is not much different from the minimum principal stress.

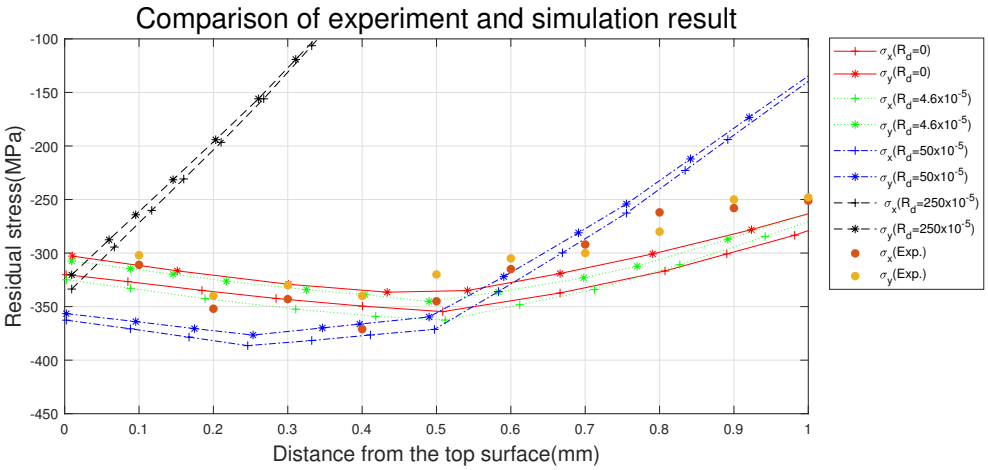

Figure 21. Residual stress comparison of the experiment and simulation result.

5. Conclusion

In this study, LSP FE simulation is conducted and from the solution, deformation and the residual stress are evaluated. Simulation result is also compared with LSP experiment specimen whether the proposed simulation process is appropriate. Summary of this study are:

- Single and Multi-shot explicit dynamic LSP FE analysis is conducted with proposed static damping model by *ANSYS Autodyn*.
- Implicit analysis which stabilizing the geometry can be skipped by adding static damping value.
- The static damping quickly settles the model after shock loading but when large damping, residual stress is formed near surface of geometry, not deeply, and relatively small plastic deformation can be obtained.
- Comparison of residual stress measurement results on LSP specimen with compressed residual stress obtained from simulation showed a similar tendency.
- With using proper static damping value in LSP FE simulation, it can reduce the calculation time even not much effect on the simulation result.

Compared to other peening methods, LSP is a high-cost material surfacing process. To evaluated the actual residual stress distribution, additional destructive test such as hold drilling is also required. Therefore, when needs to be quickly checked the residual stress distribution according to the depth formed by the LSP, the proposed FE simulation model can be appropriate.

Author Contributions: "Conceptualization, Ryoonhan Kim; methodology, Ryoonhan Kim; software, Seung-Hoon Bae, Dae-Won Cho; validation, Ryoonhan Kim and Dae-Won Cho; formal analysis, Ryoonhan Kim and Won-Geun Yi; investigation, Ryoonhan Kim and Won-Geun Yi; resources, Seung-Hoon Bae and Dae-Won Cho; data curation, Ryoonhan Kim, Won-Geun Yi; writing—original draft preparation, Ryoonhan Kim; writing—review and editing, Dae-Won Cho; supervision, Jeong Suh; project administration, Dongsig Shin; funding acquisition, Jeong Suh, Dongsig Shin and Kwang-Hyeon Lee. All authors have read and agreed to the published version of the manuscript."

Acknowledgments: This research was supported by the National Research Council of Science and Technology. (Project number: NK232A, 2021, Korea)

Conflicts of Interest: "The authors declare no conflict of interest." "The funders had no role in the design of the study; in the collection, analyses, or interpretation of data; in the writing of the manuscript, or in the decision to publish the results".

Abbreviations

FEM	Finite Element Method
LSP	Laser Shock Peening
PDE	Partial Differential Equations

References

1. Ding, K.; Ye, L. *Laser shock peening: performance and process simulation*; Woodhead Publishing, 2006.
2. Lu, J.Z.; Luo, K.Y.; Yang, D.K.; Cheng, X.N.; Hu, J.L.; Dai, F.Z.; Qi, H.; Zhang, L.; Zhong, J.S.; Wang, Q.W.; Zhang, Y.K. Effects of laser peening on stress corrosion cracking (SCC) of ANSI 304 austenitic stainless steel. *Corros. Sci.* **2012**, *60*, 145–152. doi:10.1016/j.corsci.2012.03.044.
3. Telang, A.; Gill, A.S.; Teysseyre, S.; Mannava, S.R.; Qian, D.; Vasudevan, V.K. Effects of laser shock peening on SCC behavior of Alloy 600 in tetrathionate solution. *Corros. Sci.* **2015**, *90*, 434–444. doi:10.1016/j.corsci.2014.10.045.
4. Grethlein, J.E. Keep 'Em Flying Laser Peening Keeps Aircraft Turbine Blades in Action. AMPTIAC Q., 2003, Vol. 7, pp. 3–7.
5. Kim, J.d.; SANO, Y. Laser Peening Application for PWR Power Plants. *J. Weld. Join.* **2016**, *34*, 13–18.
6. Braisted, W.; Brockman, R. Finite element simulation of laser shock peening. *Int. J. Fatigue* **1999**, *21*, 719–724. doi:10.1016/S0142-1123(99)00035-3.
7. Asghar, M.H.; Placido, F.; Naseem, S. P HYSICAL J OURNAL Characterization of reactively evaporated TiO 2 thin films as high. *Eur. Phys. JournalApplied Phys.* **2006**, *184*, 177–184. doi:10.1051/epjap.
8. Peyre, P.; Chaieb, I.; Braham, C. FEM calculation of residual stresses induced by laser shock processing in stainless steels. *Model. Simul. Mater. Sci. Eng.* **2007**, *15*, 205–221. doi:10.1088/0965-0393/15/3/002.
9. Amarchinta, H.K.; Grandhi, R.V.; Langer, K.; Stargel, D.S. Material model validation for laser shock peening process simulation. *Model. Simul. Mater. Sci. Eng.* **2009**, *17*. doi:10.1088/0965-0393/17/1/015010.
10. Amarchinta, H.K.; Grandhi, R.V.; Clauer, A.H.; Langer, K.; Stargel, D.S. Simulation of residual stress induced by a laser peening process through inverse optimization of material models. *J. Mater. Process. Technol.* **2010**, *210*, 1997–2006. doi:10.1016/j.jmatprotec.2010.07.015.
11. Hfaiedh, N.; Peyre, P.; Song, H.; Popa, I.; Ji, V.; Vignal, V. Finite element analysis of laser shock peening of 2050-T8 aluminum alloy. *Int. J. Fatigue* **2015**, *70*, 480–489. doi:10.1016/j.ijfatigue.2014.05.015.
12. Li, X.; He, W.; Luo, S.; Nie, X.; Tian, L.; Feng, X.; Li, R. Simulation and experimental study on residual stress distribution in titanium alloy treated by laser shock peening with flat-top and Gaussian laser beams. *Materials (Basel).* **2019**, *12*, 1–12. doi:10.3390/ma12081343.
13. Hu, Y.; Yao, Z.; Hu, J. 3-D FEM simulation of laser shock processing. *Surf. Coatings Technol.* **2006**, *201*, 1426–1435. doi:10.1016/j.surfcoat.2006.02.018.
14. Hu, Y.; Yao, Z. Numerical simulation and experimentation of overlapping laser shock processing with symmetry cell. *Int. J. Mach. Tools Manuf.* **2008**, *48*, 152–162. doi:10.1016/j.ijmachtools.2007.08.021.
15. Bhamare, S.; Ramakrishnan, G.; Mannava, S.R.; Langer, K.; Vasudevan, V.K.; Qian, D. Simulation-based optimization of laser shock peening process for improved bending fatigue life of Ti-6Al-2Sn-4Zr-2Mo alloy. *Surf. Coatings Technol.* **2013**, *232*, 464–474. doi:10.1016/j.surfcoat.2013.06.003.
16. BALLARD, P.; FOURNIER, J.; FABBRO, R.; FRELAT, J. RESIDUAL STRESSES INDUCED BY LASER-SHOCKS. *Le J. Phys. IV* **1991**, *01*, C3–487–C3–494. doi:10.1051/jp4:1991369.
17. Hasser, P.J.; Malik, A.S.; Langer, K.; Spradlin, T.J.; Hatamleh, M.I. An Efficient Reliability-Based Simulation Method for Optimum Laser Peening Treatment. *J. Manuf. Sci. Eng. Trans. ASME* **2016**, *138*. doi:10.1115/1.4033604.
18. Brockman, R.A.; Braisted, W.R.; Olson, S.E.; Tenaglia, R.D.; Clauer, A.H.; Langer, K.; Shepard, M.J. Prediction and characterization of residual stresses from laser shock peening. *Int. J. Fatigue* **2012**, *36*, 96–108. doi:10.1016/j.ijfatigue.2011.08.011.
19. ANSYS. Chapter 6, Explicit dynamics theory guide.
20. ANSYS. Explicit Dynamics Chapter 8 Analysis Settings ⁞ Viscosity ⁞ Bending.
21. ANSYS. ANSYS Explicit Dynamics Analysis Guide **2020**. p. 394.
22. Johnson, G.R.; Cook, W. A CONSTITUTIVE MODEL AND DATA FOR METALS SUBJECTED TO LARGE STRAINS, HIGH STRAIN RATES AND HIGH TEMPERATURES. *Proceedings 7th International Symposium on Ballistics* **1983**, pp. 541–547.
23. Zerilli, F.J.; Armstrong, R.W. Dislocation-mechanics-based constitutive relations for material dynamics calculations. *J. Appl. Phys.* **1998**, *61*, 1816. doi:10.1063/1.338024.
24. Khan, A.S.; Suh, Y.S.; Kazmi, R. Quasi-static and dynamic loading responses and constitutive modeling of titanium alloys. *Int. J. Plast.* **2004**, *20*, 2233–2248. doi:10.1016/J.IJPLAS.2003.06.005.
25. Karkalos, N.E.; Markopoulos, A.P. Determination of Johnson-Cook material model parameters by an optimization approach using the fireworks algorithm. Procedia Manuf. Elsevier B.V., 2018, Vol. 22, pp. 107–113. doi:10.1016/j.promfg.2018.03.017.
26. Langer, K.; Spradlin, T.J.; Fitzpatrick, M.E. Finite element analysis of laser peening of thin aluminum structures. *Metals (Basel).* **2020**, *10*, 1–16. doi:10.3390/met10010093.
27. Nam, T. Finite element analysis of residual stress field induced by laser shock peening. PhD thesis, Ohio State University, 2002.
28. Kim, J.S.; Nam, H.S.; Kim, Y.J.; Kim, J.H. Numerical Study of Laser Shock Peening Effects on Alloy 600 Nozzles with Initial Residual Stresses. *J. Press. Vessel Technol. Trans. ASME* **2017**, *139*, 1–8. doi:10.1115/1.4035977.

29. Berthe, L.; Fabbro, R.; Peyre, P.; Tollier, L.; Bartnicki, E. Shock waves from a water-confined laser-generated plasma. *J. Appl. Phys.* **1997**, *82*, 2826–2832. doi:10.1063/1.366113.
30. Sun, B.; Qiao, H.; Zhao, J. Accurate numerical modeling of residual stress fields induced by laser shock peening. *AIP Adv.* **2018**, *8*. doi:10.1063/1.5039674.
31. Espinosa, H.D.; Lee, S.; Moldovan, N. A novel fluid structure interaction experiment to investigate deformation of structural elements subjected to impulsive loading. *Exp. Mech.* **2006**, *46*, 805–824. doi:10.1007/s11340-006-0296-7.